

Insertion loss spectra for 2D periodic arrays of rigid or elastic cylinders with their axes parallel to a nearby surface

Anton Krynkin¹, Olga Umnova¹,
Juan Sanchez-Perez²

Alvin Y.B. Chong³, Shahram Taherzadeh³ and Keith Attenborough³

¹ Acoustics Research Centre, The University of Salford, Salford, Greater Manchester, UK

² Polytechnic University of Valencia, Spain

³ Department of Design Development Environment and Materials, The Open University, Milton Keynes, UK
email: a.krynkin@salford.ac.uk

Abstract

The acoustical performances of regular arrays of cylindrical elements with their axes aligned and parallel to a ground plane have been investigated through predictions and laboratory experiments. Semi-analytical predictions based on multiple scattering theory and numerical simulations based on Boundary Elements formulation have been made. In an anechoic chamber, 7×3 arrays of solid scatterers (hollow PVC cylinders of 55 mm diameter) have been located near to ground planes consisting of Medium Density Fibreboard (MDF) plate or sheets of porous materials. Measurements of Insertion Loss (IL) spectra have been made without and with ground planes plus arrays for several source and receiver heights. The resulting data have been compared with predictions and numerical simulations. The introduction of a ground plane is shown to have noticeable influences on free field IL spectra. The effects are most adverse when the frequencies of the band gaps coincide with the minima in the excess attenuation spectrum due to the ground alone. On the other hand if the ground effect excess attenuation minimum coincides with an array pass band then it is retained in the insertion loss. Cases are identified where it is possible to obtain an insertion loss with the array in the presence of ground that is greater than that of the same array in the free field.

1 Introduction

Periodic arrangements of acoustic scatterers embedded in a medium with different physical properties give rise to ranges of frequencies, known as band gaps, where the transmission of acoustic waves is forbidden. If the scatterers are solid and the embedding medium is air then these arrays are called Sonic Crystals (SC). There is interest in the potential use of sonic crystals as environmental noise barriers. A semi-analytical approach for predicting

the transmission properties of sonic crystals has been developed for circular scatterer cross-sections and is based on the superposition of the solution for a single scatterer [1, 2, 3, 4]. However, this scattering approach predicts their acoustical performance in the absence of a ground plane. Clearly this is unrealistic for environmental noise barriers. Although the most interesting situation is likely to involve periodic vertical cylinder arrays, this would require solution of a 3D problem. Here are considered the more tractable problem involving a periodic array of cylinders with their axes parallel to the ground.

If the ground can be considered to be acoustically-rigid, the multiple scattering method can be modified using the method of images to construct the reflected field [5]. For finite impedance ground, it is necessary also to modify the scattered field, i.e. the waves scattered by the ground, to satisfy boundary conditions on the ground [6, 7]. Numerical approaches can allow for more complex geometries. The Boundary Element Method (BEM) based on the integral equations method is the most common of these. Specifically it is possible to modify the Green's function [8] so that the domain with impedance ground transforms into the unbounded acoustic medium. The result is that the boundary integral equations are only considered over the surface of the scatterers. With this approach the computational time can be relatively low compared to that for the full problem with the ground as an additional surface. The method has been widely used to predict the performance of the noise barriers mounted on the ground [9, 10].

These semi-analytical and numerical methods are used to analyse the performance of arrays of rigid or elastic cylindrical scatterers suspended with their axes parallel to a rigid or finite impedance ground. In this paper two square array of 5x3 and 7x3 scatterers are considered. The former is used to validate the developed semi-analytical and numerical models whereas the performance of the latter is compared with the experimental results. The predicted performance of the sonic crystals in the presence of rigid ground is compared with that of the crystals placed in the free field. Experiments have been carried out in an anechoic chamber and the resulting insertion loss data are compared with predictions. It is shown how the presence of the impedance ground affects the maxima of positive insertion loss for sonic crystals associated with so-called band-gaps.

The analytical and numerical approaches are outlined and some of the resulting predictions are discussed in section 2. The experiments are described in section 3. Predictions and data are compared and discussed in section 4 before concluding remarks are made in section 5.

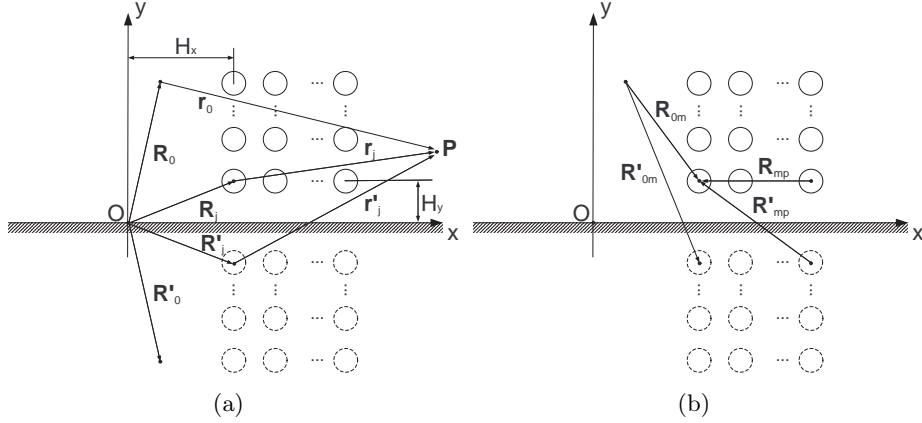


Figure 1: Square lattice array above a perfectly reflecting plane. (a) Set of vectors used in equation (4). (b) Set of vectors used in equation (7).

2 Analytical and numerical formulations

2.1 Multiple scattering

2.1.1 Rigid scatterers

Consider a point source and an array of M circular scatterers placed in a (positive) half-space (Figure 1) characterised by the sound speed in air $c = 344$ m/s and density $\rho = 1.2$ kg/m³. The position of each scatterer C_m , $m = 1..M$ is given by the vector \mathbf{R}_m . The image of scatterer C_m is defined by the radius vector \mathbf{R}'_m . The scatterers are considered to be arranged in a square lattice which is defined by the lattice constant L .

The solution of the appropriate scattering problem satisfies the Helmholtz equation in the half-space that is written in polar coordinates (r, θ) as

$$\Delta p(\mathbf{r}) + k^2 p(\mathbf{r}) = 0, \quad (1)$$

where $\Delta = \frac{1}{r} \frac{\partial}{\partial r} \left(r \frac{\partial}{\partial r} \right) + \frac{1}{r^2} \frac{\partial^2}{\partial \theta^2}$, $\mathbf{r} = r(\cos \theta, \sin \theta)$ is the radius vector, p is acoustic displacement potential, $k = \omega/c$, ω is angular frequency. Equation (1) is solved in conjunction with radiation conditions

$$\frac{\partial p}{\partial r} - ikp = o(r^{-1/2}), \text{ as } r \rightarrow \infty, \quad (2)$$

and with the Neumann condition imposed on the boundary of acoustic half-space (i.e. rigid ground) and on the surface of the scatterers (this condition has to be replaced by continuity conditions if scatterer is an elastic shell [12]) that is

$$\frac{\partial p}{\partial n} = 0, \quad (3)$$

Using the multiple scattering technique [3, 11] and method of images [5] the general solution of the formulated problem can be written as [13]

$$p(\mathbf{r}) = p_0(\mathbf{r}) + p_s(\mathbf{r}), \quad (4)$$

within which point source and scattered fields are given by

$$\begin{aligned} p_0(\mathbf{r}) &= H_0^{(1)}(kr_0) + H_0^{(1)}(kr'_0), \\ p_s(\mathbf{r}) &= p_{s,d}(\mathbf{r}) + p_{s,r}(\mathbf{r}), \\ p_{s,d}(\mathbf{r}) &= \sum_{m=1}^M \sum_{n=-\infty}^{+\infty} A_n^m Z_n^m H_n^{(1)}(kr_m) e^{in\theta_m}, \\ p_{s,r}(\mathbf{r}) &= \sum_{m=1}^M \sum_{n=-\infty}^{+\infty} A_n^m Z_n^m H_n^{(1)}(kr'_m) e^{-in\theta'_m}, \end{aligned} \quad (5)$$

respectively, and where $\mathbf{r}_0 = r_0(\cos \theta_0, \sin \theta_0)$ is the vector connecting the point source and the receiver point (i.e. point P in Figure 1), $\mathbf{r}_m = r_m(\cos \theta_m, \sin \theta_m)$ is vector connecting the centre of scatterer C_m and the receiver and prime (') marks the geometrical parameters for the image source and the image scatterers placed in the negative half-space. The solution for the unbounded acoustic space can be retrieved from equation (4) by putting to zero all terms related to the constructed images. One can also deduce from equation (4) that for the source and receiver both on the ground the acoustic pressure in a half-space equals to the doubled pressure in the unbounded acoustic space.

The factors describe the type of conditions imposed on the surface of the scatterers and in case of rigid cylinders they can be expressed as

$$Z_n^m = \frac{\partial_r J_n(ka_m)}{\partial_r H_n^{(1)}(ka_m)}. \quad (6)$$

where a_m is the radius of scatterer C_m and ∂_r is the derivative with respect to polar coordinate r .

Applying the addition theorem [15, 16], described in Appendix, to the solution (4) and substituting it to the boundary condition (3), the algebraic system of equations can be derived to find the unknown coefficients A_n^m . This system is given by

$$\begin{aligned} A_n^m + \sum_{q=-\infty}^{\infty} \left\{ \sum_{p=1, p \neq m}^M A_q^p Z_q^p H_{q-n}^{(1)}(kR_{mp}) e^{i(q-n)(\pi+\alpha_{mp})} + \sum_{p=1}^M A_q^p Z_q^p H_{q+n}^{(1)}(kR'_{mp}) e^{-i(q+n)\alpha'_{mp}+iq\pi} \right\} \\ = -H_n^{(1)}(kR_{0m}) e^{-in(\pi+\alpha_{0m})} - H_n^{(1)}(kR'_{0m}) e^{-in(\pi+\alpha'_{0m})}, \quad n \in \mathbb{Z}, \quad m = 1..M. \end{aligned} \quad (7)$$

where vector $\mathbf{R}_{0m} = R_{0m}(\cos \alpha_{0m}, \sin \alpha_{0m})$ defines the position of scatterer C_m with respect to point source and vector $\mathbf{R}_{mp} = R_{mp}(\cos \alpha_{mp}, \sin \alpha_{mp})$ defines the position of scatterer C_p with respect to scatterer C_m . Note that system of equations (7) can be transformed to that for the case of unbounded acoustic space by eliminating all terms dependent on the geometrical parameters of image source and scatterers.

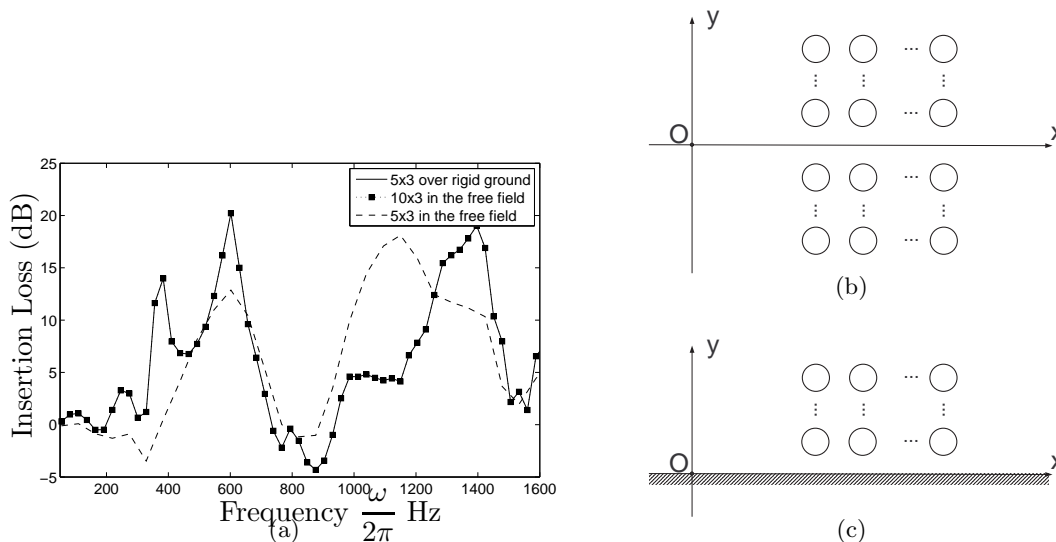


Figure 2: (a) Predicted insertion loss spectra with source and receiver coordinates of (0,0) and (10,0) respectively and the nearest part of the array at $H_x = 1.5$ m from the source (i) for a 5×3 square array of rigid cylinders with diameter 0.1 m, lattice constant 0.3 m in the free field and 'lowest' cylinder centers at $H_y = 0.15$ (ii) for this lattice above acoustically-rigid plane at $y = 0$ and (iii) for a doubled (i.e. a 10×3) lattice in the free field (b) schematic of the 10×3 array, consisting of the original 5×3 array plus its 'mirror image', and (c) schematic of the 5×3 array over rigid ground.

In Figure 2, the predicted insertion loss spectrum due to a 5×3 array of rigid scatterers over an acoustically-rigid ground is compared with those obtained (a) for the same array in free field conditions and (b) for an array of double the size (10×3) in free field conditions. Note that throughout this paper the insertion loss is calculated as

$$IL = 20 \log_{10} \left| \frac{p_0}{p} \right|. \quad (8)$$

The cylinders locations in the lower half of the 10×3 array are defined by the coordinates of the image cylinders in the perfectly reflecting plane. The distance to the ground, 0.15 m, of the centers of the lowest cylinders in the array is half of the lattice constant $L = 0.3$ m so that they are separated from the centers of the cylinders of the image array nearest

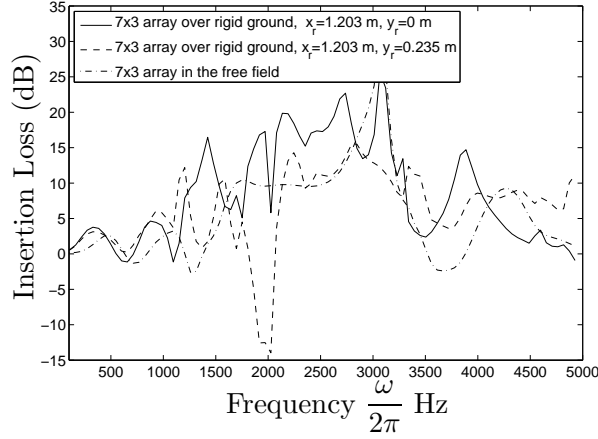


Figure 3: Predicted insertion spectra for source at coordinates (0,0.235) m and 0.755 m from a 7×3 array of rigid cylinders with $L = 0.069$ m (i) over acoustically-rigid ground with receiver coordinates (1.203,0) m (solid black line) (ii) over acoustically-rigid ground with receiver coordinates (1.203,0.235) (broken line) and (iii) in free field (dash-dot line).

the ground plane by the lattice constant. With the source and receiver on the ground, the predicted insertion loss spectrum of the 5×3 array in the presence of the rigid ground is the same as that predicted for an array of double the size (10×3) in the free field. It is also observed that insertion loss of 5×3 array in half-space may be higher than that for the same size of the array in the unbounded acoustic space. This is true particularly for the predicted maxima of insertion loss related to the first Bragg band gap near 573 Hz.

Figure 3 compares predicted insertion loss spectra for source at coordinates (0,0.235) m and 0.755 m from a 7×3 array of rigid cylinders with $L = 0.069$ m (a) over acoustically-rigid ground with receiver coordinates (1.203,0) m, (b) over acoustically-rigid ground with receiver coordinates (1.203,0.235) m and (c) in free field. The predicted effect of raising the receiver is clearly detrimental to insertion loss at frequencies corresponding to the (rigid) ground effect dip.

2.1.2 Elastic shell scatterers

A multiple scattering analysis can be carried out to predict the insertion loss spectrum due to an array of elastic shells with their axes parallel to a rigid ground. The identical elastic shells are characterised by density ρ_s , Young's modulus E , Poisson's ratio ν , shear velocity c_2 , half-thickness h and the mid-surface radius S . For certain ranges of values of these parameters, the first elastic shell resonance (i.e. the axisymmetric resonance) can be observed below the first Bragg band gap associated with the lattice constant of the array in the unbounded acoustic space. This results in additional positive insertion loss peaks [12].

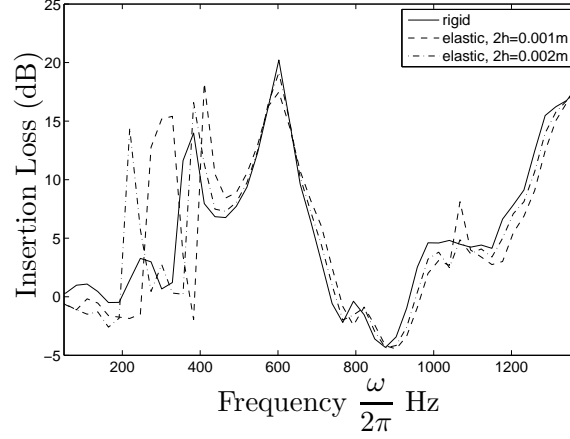


Figure 4: Predicted insertion loss spectra for the source-receiver-array (5×3) geometry specified for Figure 2(c) in the presence of acoustically-rigid ground at $y = 0$, with rigid cylinders (solid line), elastic shells ($\rho_s = 1100\text{kg/m}^3$, $E = 1.75\text{ MPa}$, $\nu = 0.4998$, $c_2 = 23\text{ m/s}$) with wall thickness 0.001 m (broken line) and elastic shells with wall thickness 0.002 m (dot-dash line).

The asymptotic theory of thin elastic shells [17] has been used [12, 13] to derive the factors

$$Z_n^m = \frac{\partial_r J_n(kS)}{\partial_r H_n^{(1)}(kS) + iU_n}, \quad (9)$$

where

$$U_n = \frac{\epsilon}{\kappa \pi S h} \frac{n^2 - k_3^2 S^2}{(1 + n^2 - k_3^2 S^2) \partial_r J_n(kS)}. \quad (10)$$

and $\epsilon = \rho c / (\rho_s c_2)$ is the relative impedance, $\kappa = c / c_2$ and $k_3 = \omega \sqrt{\rho(1 - \nu^2)/E}$. This new form of the factor Z_n^m can easily be transformed to that for the rigid cylinder assuming that relative impedance $\epsilon \rightarrow 0$. Note that multiple scattering technique can be easily adapted to arrangements of circular scatterers varied in size and type of surface (such as rigid and elastic wall).

Figure 4 compares the predicted insertion loss spectra of the array of elastic shells in the acoustic half-space with that of the array of rigid shells. Additional insertion loss peaks due to axisymmetric resonances of the elastic shells are observed below the peak related to the Bragg band gap. Increasing the shell thickness is predicted to reduce the frequency of the axisymmetric resonance.

Figure 5 compares insertion loss spectra for 7×3 rigid cylinder and elastic shell arrays with lattice constant $L = 0.069\text{ m}$ above acoustically-rigid ground with different receiver heights. The predicted effect of thin elastic shell in Figure 4 is affected by the ground effect dip. In Figures 5(a) and (b) the additional peak due to the axisymmetric resonance of the

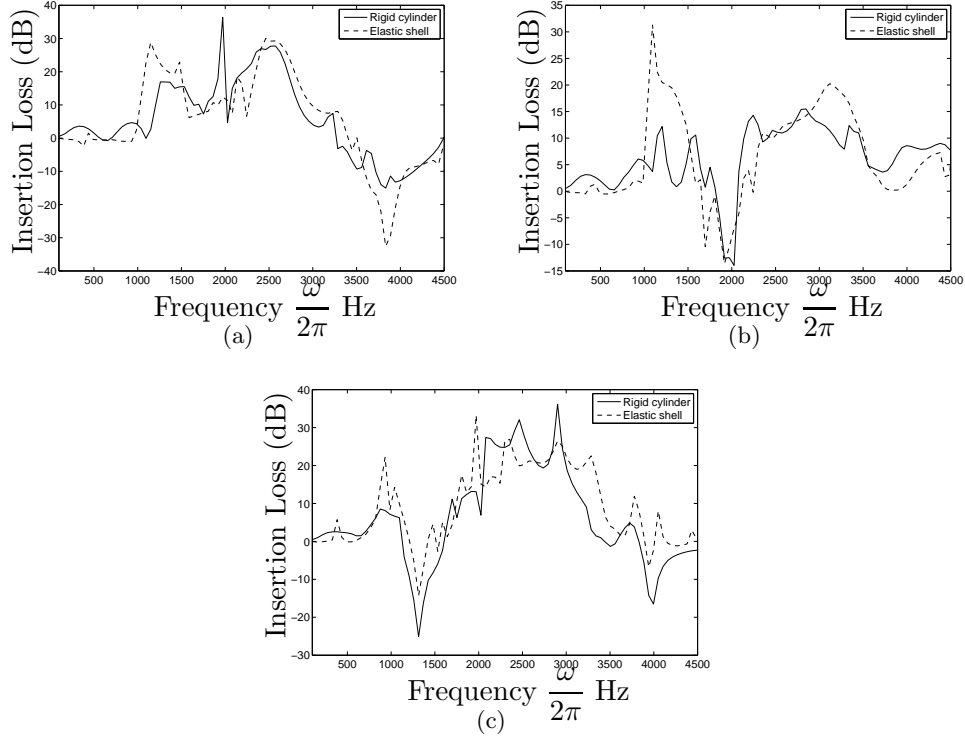


Figure 5: Predicted insertion loss spectra for source at coordinates $(0,0.235)$ m and 0.755 m from a 7×3 array of (i) rigid cylinders of diameter 0.055 m (solid black line) and (ii) elastic shells of diameter 0.055 m and thickness 0.00025 m (broken line) over acoustically-rigid ground with receiver coordinates (a) $(1.203,0.117)$ m, (b) $(1.203,0.235)$ m and (c) $(1.203,0.352)$ m. Arrays of cylinders placed near to a ground surface. The elastic shell is made of latex with material parameters specified in Figure 4.

shell appear around 1200 Hz. On the other hand this peak does not exist when receiver is raised to the point (1.203,0.352) m in Figure 5 so that ground effect dip arrives in the vicinity of axisymmetric resonance.

2.2 Calculations based on the boundary integral equation

The influence of finite impedance ground on insertion loss has been calculated by solving the boundary integral equation formulated for an array of rigid scatterers.

The Laplacian in equation (1) is rewritten in terms of (x, y) coordinates using $\Delta = \partial^2/\partial x^2 + \partial^2/\partial y^2$.

The boundary condition imposed on the ground surface is written as

$$\frac{\partial p}{\partial n} - ik\beta p = 0, \quad (11)$$

where β is admittance of the homogeneous impedance plane [8, eq. (1.2.11)].

Then, applying relations (1),(2) and (11) to the Green's theorem [18] the integral equation for $p(\mathbf{r})$ can be derived in the following form [13, 14]

$$\epsilon(\mathbf{r})p(\mathbf{r}) = G_\beta(\mathbf{r}_0, \mathbf{r}) + \sum_{m=1}^M \int_{\partial C_m} \frac{\partial G_\beta(\mathbf{r}_s, \mathbf{r})}{\partial n(\mathbf{r}_s)} p(\mathbf{r}_s) ds, \quad (12)$$

where

$$\epsilon(\mathbf{r}) = \begin{cases} 1, & \mathbf{r} \notin \bar{C}_m \\ 1/2, & \mathbf{r} \in \partial C_m \end{cases} \quad (13)$$

with $\mathbf{r} = (x, y)$, $G_\beta(\mathbf{r}_0, \mathbf{r})$ is the solution for the half-space in the absence of the scatterers [8, eq. (2.1.2)] and ∂C_m is the surface of scatterer C_m . Note, that in relation (13) the corner points of an obstacle are not defined due to the circular shape of the scatterers.

Figure 6 demonstrates that the boundary integral formulation yields results close to those obtained using multiple scattering theory for an array of horizontal cylinders above acoustically-rigid ground.

The increasing difference in the predictions at higher frequencies can be reduced by taking more elements on the surface of the scatterers. This however increases the computational time.

Figure 7 shows predictions obtained using the boundary integral formulation for three values of ground impedance based on a one parameter (effective flow resistivity) impedance model [19]. The predicted insertion loss spectrum for the lowest value of effective flow resistivity (20 kPas/m² corresponding to a mineral wool) shows more or less complete elimination the band-gap effect whereas the predicted insertion loss spectra for the higher flow resistivities (168 kPas/m² and 250 kPas/m² corresponding to soil and grassland respectively), indicate that the presence of a relatively acoustically-rigid surface maintains

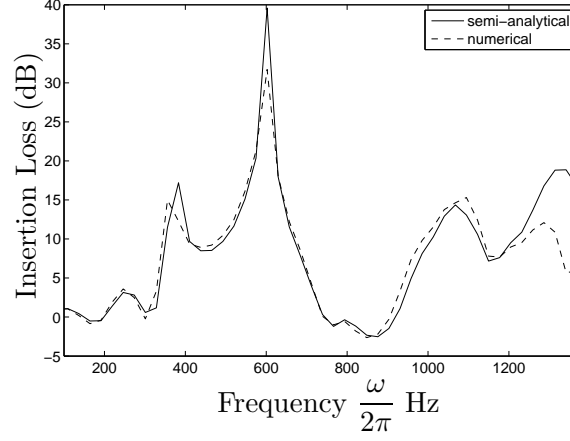


Figure 6: Predicted (scattering theory - solid line; boundary element calculation - broken line) insertion loss spectra for a square 5×3 array of rigid scatterers of radius 0.1 m with lattice constant $L = 0.3$ m above an acoustically-rigid ground. The source coordinates (0,0) are on the ground and 1.5 m from the center of the front column of cylinders. The centers of the lowest cylinders are at a height of 0.15 m. The point of observation is at (10,0.45) m

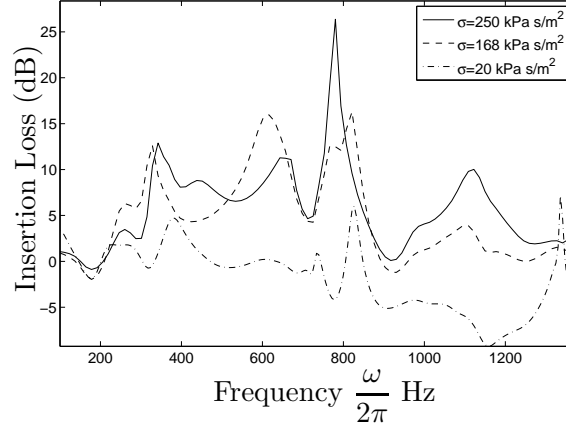


Figure 7: Insertion loss spectra predicted for a square 5×3 array of rigid scatterers of radius 0.1 m with lattice constant $L = 0.3$ m. The source coordinates (0,0) m are on the ground and 1.5 m from the center of the front column of cylinders. The centers of the lowest cylinders are at a height of 0.15 m. The coordinates of the receiver point are (10,0.45) m. The solid, broken and dash-dot lines correspond to the different values of effective flow resistivity in the key.

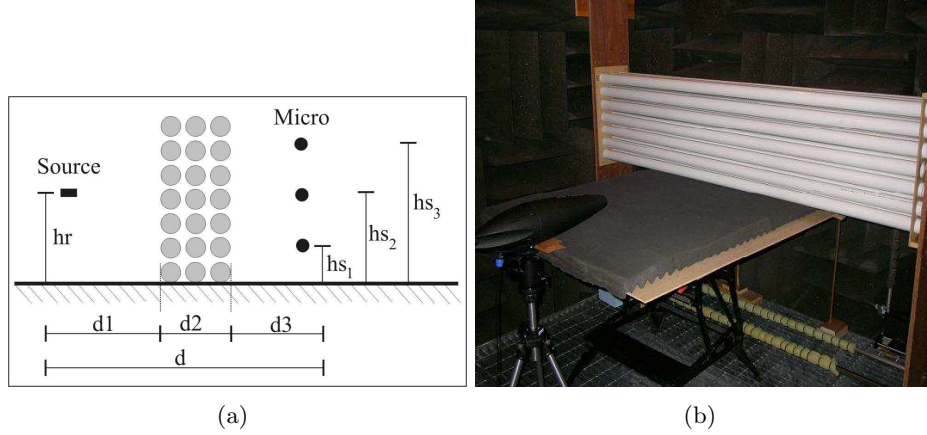


Figure 8: (a) plan of source, receiver and array (b) 7×3 array of PVC pipe over MDF board covered with open cell foam layer in the anechoic chamber.

the improved performance of the sonic crystals in the frequency intervals related to the band-gaps.

Alternative to BEM could be the approach based on Weyl-Van der Pol formula modeling locally reacting ground [20]. This approach was employed in [21, 22] for the single scatterer. However its application to the array of scatterers is heuristic and can only be used within the limited range of source-array and array-receiver distances. As an example in Appendix B it is shown that the results deteriorates with the increase of the receiver distance to the ground.

3 Laboratory experiment

2 m PVC pipes have been used as the rigid cylinders with outer diameters of 55 mm. The sound source was a Bruel & Kjaer point source loudspeaker controlled by a Maximum-Length Sequence System Analyzer (MLSSA) system enabling determination of impulse responses. Measurements of the insertion loss (IL) spectra for and arrays of cylinders placed near to a ground surface in an anechoic chamber. Figures 8 (a) and (b) show example measurement arrangements. Supports for the 2 m long cylinders were provided by holed MDF boards at the top and base of each array.

A 0.03 m thick MDF board large enough to avoid the diffraction at the edges was used as a rigid surface. As shown in Figure 8(a), the loudspeaker point source was positioned 0.755 m from the array at the height of the horizontal mid-plane of the array (0.23 m above the ground). The height of the receiver microphone was 0.117 m, 0.235 m or 0.352 m and it was placed in a vertical plane 0.257 m from the back of the array. The receiver heights were chosen to be below, at, and above, the horizontal mid-plane of the array. In

all cases, of distance between the microphone and the SCNB has been considered. The difference between the sound levels recorded in the X direction (0°) at the same point with and without the ground plus the array was measured [23].

4 Comparisons between data and predictions

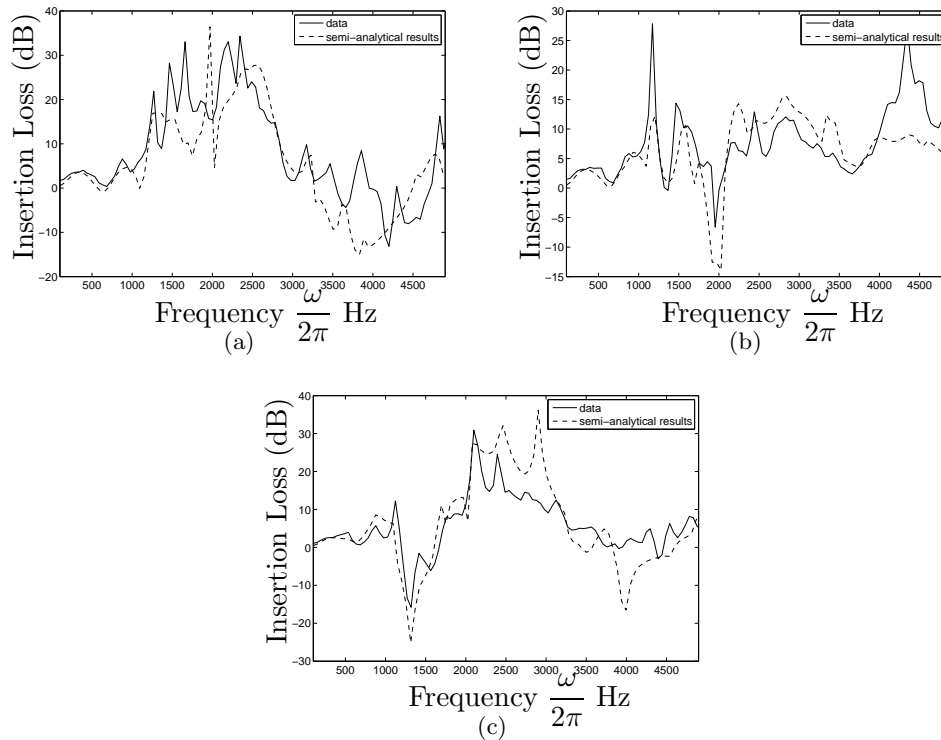


Figure 9: Measured (solid line) and predicted (broken line) insertion loss spectra for source at coordinates (0,0.235) m and 0.755 m from a 7×3 array of rigid cylinders of diameter 0.055 m over acoustically-rigid ground with receiver coordinates (a) (1.203,0.117) m, (b) (1.203,0.235) m and (c) (1.203,0.352) m. Arrays of cylinders placed near to a ground surface.

Figure 9 compares measured and predicted insertion loss spectra for 7×3 rigid cylinder arrays over rigid ground for three receiver heights using the source location described in section 3. The agreement between predictions and measurements is fairly good. Both data and predictions for the elevated receiver heights show the adverse influences of the (rigid) ground effect on the IL spectra near 2000 Hz and 1250 Hz for receiver heights of 0.235 m and 0.352 m respectively. In Figures 9(a) and (c) wide positive IL peak around 2500 Hz can

be related to the effect of Bragg band gap observed for the array in the unbounded acoustic space. However, in immediate proximity of the ground effect this positive performance of the structure is destroyed as it is shown in Figure 9(b).

Figure 10 compares corresponding measured and predicted insertion loss spectra for 7×3 rigid cylinder arrays over finite impedance ground for three receiver heights using the source location described in section 3. In this case the finite impedance (open cell foam layer) surface is represented by a two parameter impedance model [24] with $\sigma_e = 4 \text{ kPa s/m}^2$, $\alpha_e = 105 \text{ m}^{-1}$. Again the agreement between predictions and measurements is fairly good. The adverse influences of ground effect on the IL spectra are shifted towards lower frequencies. It is also noted that due to this shift in the ground effect the positive IL peaks related to the Bragg band gap can be observed for all three positions of the receiver.

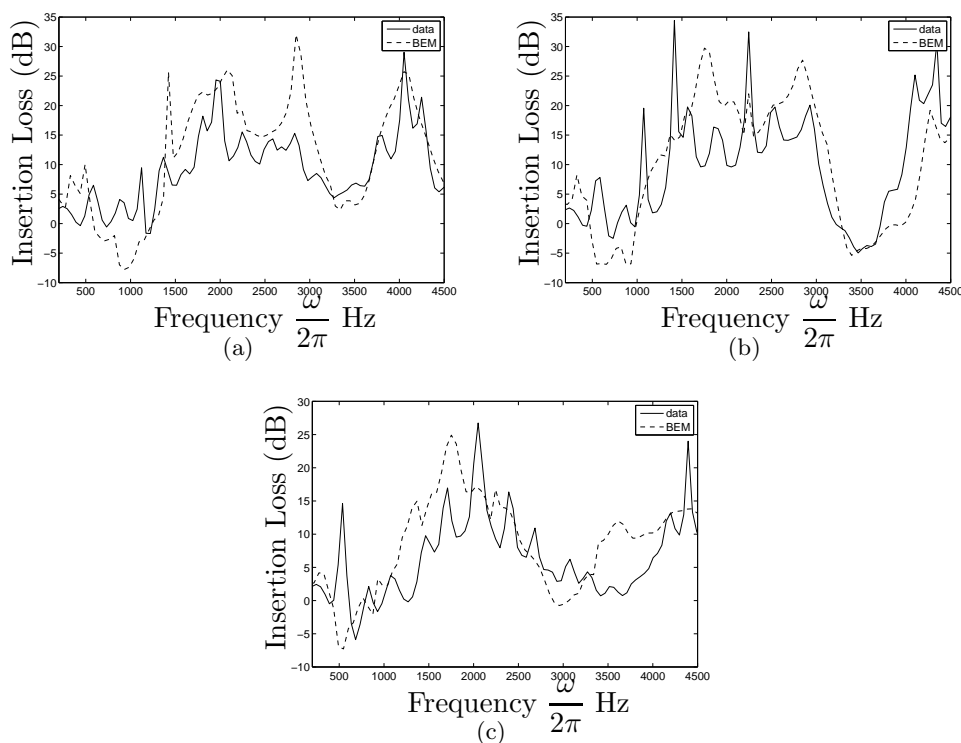


Figure 10: Measured (solid line) and predicted (broken line) insertion loss spectra for source at coordinates (0,0.235) m and 0.755 m from a 7×3 array of rigid cylinders of diameter 0.055 m over finite impedance ground with receiver coordinates (a) (1.203,0.117) m, (b) (1.203,0.235) m and (c) (1.203,0.352) m. Arrays of cylinders placed near to a ground surface.

5 Concluding remarks

In this paper the semi-analytical model is derived for predicting multiple scattering effects of the finite array over the rigid ground. The results are validated by the numerical technique, namely BEM, and compared with the data. It is shown that performance of the array in the half-space is similar to the doubled array in the unbounded acoustical space. The influence of the rigid ground can destroy positive performance of the structure related to the Bragg band gap. However introduction of the impedance ground can shift this influence to the lower frequencies and, as a result, restore the effect of the Bragg band gap. In case of the impedance ground numerical technique BEM is compared with the alternative semi-analytical approach based on the Weyl–Van der Pol formula. The results show that approximation of the impedance ground in the semi-analytical approach brakes down with the change of the receiver position.

Acknowledgment

This work was supported by the UK Engineering and Physical Sciences Research Council (grant EP/E063136/1) and by MEC (Spanish Government) and FEDER funds, under Grant No. MAT2009-09438.

Appendix A: Graf’s addition theorem

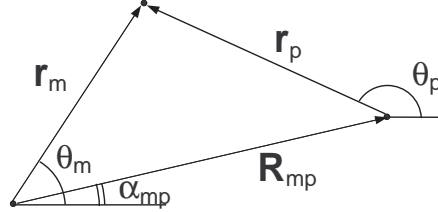


Figure 11: Geometry for Graf’s addition theorem.

In this section Graf’s addition theorem is modified so that it can be applied to the solution of the reflected scattered field $p_{s,r}$ in equation (4). First the addition theorem is stated for the solution of the direct scattered field $p_{s,d}$, yielding

$$H_n^{(1)}(kr_p)e^{in\theta_p} = \sum_{q=-\infty}^{\infty} J_q(kr_m)H_{n-q}^{(1)}(kR_{mp})e^{i(n-q)(\pi+\alpha_{mp})}e^{iq\theta_p}, \quad (14)$$

for $r_m < R_{mp}$, $m \in \mathbb{Z}$. The outlined form of the additional theorem is based on the configuration shown in Figure 11. To adapt theorem (14) to solution $p_{s,r}$ the index n has to

be replaced by its negative counterpart $n = -n$. Using the relation $H_{-n}^{(1)}(z) = e^{in\pi} H_n^{(1)}(z)$ the addition theorem is written as

$$H_n^{(1)}(kr_p)e^{-in\theta_p} = \sum_{q=-\infty}^{\infty} J_q(kr_m)H_{n+q}^{(1)}(kR_{mp})e^{-i(n+q)\alpha_{mp}+in\pi}e^{iq\theta_p}, \quad (15)$$

The latter can be used in equation (4) to transform image solution to that defined by the variables of the real scatterer.

Appendix B: Spherical reflection coefficient

The Weyl–Van der Pol formula [20] can be used to predict impedance ground effect. For the case of line source over the impedance ground the acoustic wave field is approximated by well-known formula [22] that is

$$p_0(\mathbf{r}) = H_0^{(1)}(kr_0) + Q_0 H_0^{(1)}(kr'_0). \quad (16)$$

By the analogy with the source over the ground the scattered wave field for the array of circular scatterers can be written as

$$p_s(\mathbf{r}) = \sum_{m=1}^M \sum_{n=-\infty}^{+\infty} A_n^m Z_n^m \left[H_n^{(1)}(kr_m)e^{in\theta_m} + Q_m H_n^{(1)}(kr'_m)e^{-in\theta'_m} \right]. \quad (17)$$

This solution is rather heuristic approach of predicting multiple scattering over the impedance ground and its accuracy depends very much on the position of the receiver. The spherical wave reflection coefficient Q_m , $m = 0..M$, is given by

$$Q_m = V_m + (1 - V_m)F(w_m) \quad (18)$$

where

$$\begin{aligned} V_m &= \frac{\cos \alpha_m - \beta}{\cos \alpha_m + \beta} \\ w_m &= \sqrt{\frac{ikr'_m}{2}}(\cos \alpha_m + \beta) \\ F(w_m) &= 1 + i\sqrt{\pi}w_m \exp(-w_m^2) \operatorname{erfc}(-iw_m) \end{aligned} \quad (19)$$

within which α_m is the angle of incidence defined by either position of the source or centre of the scatterer [22].

In Figure 12 the predictions based on (a) BEM and (b) semi-analytical approach described by equations (4) and (16)-(19) are compared with the measured insertion loss for 7x3 array of rigid scatterers over the impedance ground with the parameters taken from

section 4. Figure 12(a) shows that semi-analytical results are in good agreement with the data if the receiver is close to the ground. For the receiver raised to the higher positions Figures 12(b) and (c) demonstrate unwanted effects observed for the semi-analytical approach around 4000 Hz and 2500 Hz respectively. In the frequency range where these effects are observed the numerical approach such as BEM gives better agreement with the data and preferable for predicting acoustic effects of multiple scattering by a finite periodic array.

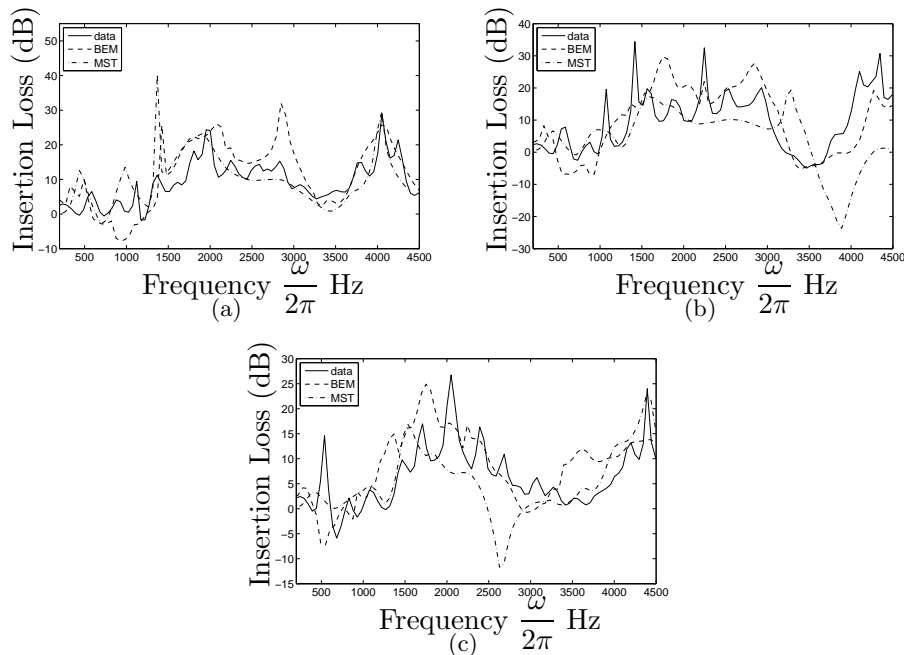


Figure 12: Measured (solid line), predicted with BEM (broken line) and predicted with Weyl–Van der Pol formula (dash-dot line) insertion loss spectra for source at coordinates (0,0.235) m and 0.755 m from a 7×3 array of rigid cylinders of diameter 0.055 m over finite impedance ground with receiver coordinates (a) (1.203,0.117) m, (b) (1.203,0.235) m and (c) (1.203,0.352) m. Arrays of cylinders placed near to a ground surface.

References

- [1] J.V. Sanchez-Perez, C. Rubio, R. Martinez-Sala, R. Sanchez-Grandia and V. Gomez, “Acoustic barriers based on periodic arrays of scatterers”, *Applied Physics Letters*, **81**, 5240–5242 (2002).

- [2] J. V. Sanchez-Perez, D. Caballero, R. Martinez-Sala, C. Rubio, J. Sanchez-Dehesa, F. Meseguer, J. Llinares, and F. Galvez, “Sound Attenuation by a Two-Dimensional Array of Rigid Cylinders”, *Physical Review Letters* **80**, 5325-5328 (1998).
- [3] C.M. Linton and D.V. Evans, “The interaction of waves with arrays of vertical circular cylinders”, *Journal of Fluid Mechanics*, **215**, 549–569 (1990).
- [4] O. Umnova, K. Attenborough and C.M. Linton, “Effects of porous covering on sound attenuation by periodic arrays of cylinders”, *The Journal of the Acoustical Society of America*, **119**, 278–284 (2006).
- [5] P. Boulanger, K. Attenborough, Q. Qin and C.M. Linton, “Reflection of sound from random distributions of semi-cylinders on a hard plane: models and data”, *Journal of Physics D: Applied Physics*, **38**, 3480–3490 (2005).
- [6] K.M. Li, W.K. Lui and G.H. Frommer, “The diffraction of sound by an impedance sphere in the vicinity of a ground surface”, *The Journal of the Acoustical Society of America*, **115**, 42–56 (2004).
- [7] R. Borghi, F. Gori, M. Santarsiero, F. Frezza and G. Schettini, “Plane-wave scattering by a set of perfectly conducting circular cylinders in the presence of a plane surface”, *Journal of the Optical Society of America A*, **13**, 2441–2452 (1996).
- [8] S.N. Chandler-Wilde, *Ground Effects in environmental sound propagation*, PhD thesis, v.1, 1988, p. 67.
- [9] D.H. Crombie and D.C. Hothersall, “The performance of multiple noise barriers”, *Journal of Sound and Vibration*, **176**, 459–473 (1994).
- [10] D.H. Crombie, D.C. Hothersall and S.N. Chandler-Wilde, “Multiple-Edge Noise Barriers”, *Applied Acoustics*, **44**, 353–367 (1995).
- [11] F. Zavisla, “The deflection of electro magnetic waves on parallel, infinite long orbital cylinder”, *Annalen der Physik*, **40**, 1023–1056 (1913).
- [12] A. Krynkin, O. Umnova, A.Y.B. Chong, S. Taherzadeh, and K. Attenborough, “Predictions and measurements of sound transmission through a periodic array of elastic shells in air”, *Journal of the Acoustical Society of America*, **128**, 3496-3506 (2010).
- [13] A. Krynkin, O. Umnova, “On performance of Sonic Crystals in presence of ground plane”, *Proceedings of Inter-noise*, Lisbon, 2010.
- [14] A. Krynkin, O. Umnova, “The effect of ground on performance of Sonic Crystal Noise barriers”, *Proceedings of Euronoise*, Edinburgh, 2009.

- [15] M. Abramowitz and I.A. Stegun, Handbook of Mathematical Functions, National Bureau of Standards, Washington, 1964, p. 255.
- [16] P.A. Martin, Multiple Scattering: Interaction of Time-Harmonic Waves with N Obstacles, Cambridge University Press, Cambridge, 2006, p. 39.
- [17] J.D. Kaplunov, L.Yu. Kossovich and E.V. Nolde, Dynamics of thin walled elastic bodies, Academic Press, London, 1998, p.110.
- [18] R.F. Millar, “Scattering by a grating”, Canadian Journal of Physics, **39**, 81–103 (1998).
- [19] M.E. Delany and E.N. Bazley, “Acoustical properties of fibrous absorbent materials”, Applied Acoustics, **3**, 105–116 (1970).
- [20] K. Attenborough, K.M. Li and K. Horoshenkov, Predicting Outdoor Sound, Taylor & Francis, London, 2007, p. 41.
- [21] S. Hasheminejad and M. Azarpeyvand, “Modal vibrations of an infinite cylinder in an acoustic half-space”, International Journal of Engineering Science, **41**, 2253–2271 (2003).
- [22] W.K. Lui and K.M. Li, “The scattering of sound by a long cylinder above an impedance boundary”, Journal of the Acoustical Society of America, **127**, 664–674 (2010).
- [23] A.Y.B. Chong, K. Attenborough and S. Taherzadeh. “The performance of vertical and horizontal Sonic Crystal noise barriers above a ground surface”, Proceedings of Inter-noise, Lisbon, 2010.
- [24] S. Taherzadeh and K. Attenborough, “Deduction of ground impedance from measurements of excess attenuation spectra”, The Journal of the Acoustical Society of America, **105**, 2039–2042 (1999).